Dalton Transactions

The Loading of Coordination Complex Modified Polyoxometalate Nanobelts on Activated Carbon Fiber: a Feasible Strategy to Obtain Visible Light Active and High Efficient Polyoxometalate Based Photocatalyst

Journal:	*Dalton Transactions*
Manuscript ID:	DT-ART-10-2014-003092.R2
Article Type:	Paper
Date Submitted by the Author:	19-Nov-2014

Complete List of Authors:	Lu, Tingting; Inorganic Institution, Chemistry Department xu, xinxin; Inorganic Institution, Chemistry Department li, huili; Analytic and Testing center, Research Academy Li, Zhenyu; Inorganic Institution, Chemistry Department Zhang, Xia; Northeastern university, Chemistry Ou, Jinzhao; Northeastern university, Chemistry Mei, Mingliang; Northeastern university, Chemistry

The Loading of Coordination Complex Modified Polyoxometalate Nanobelts on Activated Carbon Fiber: a Feasible Strategy to Obtain Visible Light Active and High Efficient Polyoxometalate Based Photocatalyst

Tingting Lu[a], Xinxin Xu*[a], Huili Li[b], Zhenyu Li[a], Xia Zhang*[a], Jinzhao Ou[a], Mingliang Mei[a]

[a] *Department of Chemistry, College of Science, Northeast University, Shenyang, Liaoning, 110819, People's Republic of China*

[b] *Analytic and Testing center, Research Academy, Northeast University, Shenyang, Liaoning, 110819, People's Republic of China*

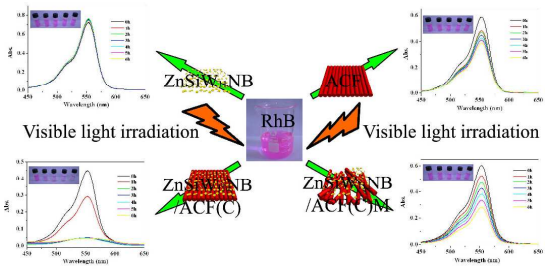

NCC/POM/ACF was fabricated successfully, which displays very excellent photocatalytic activity in visible light. Furthermore, the effect of mass ration between **NCC/POM** and **ACF** on photocatalytic activity was discussed.

The Loading of Coordination Complex Modified Polyoxometalate Nanobelts on Activated Carbon Fiber: a Feasible Strategy to Obtain Visible Light Active and High Efficient Polyoxometalate Based Photocatalyst

Tingting Lu[a], Xinxin Xu*[a], Huili Li[b], Zhenyu Li[a], Xia Zhang*[a], Jinzhao Ou[a], Mingliang Mei[a]

[a] *Department of Chemistry, College of Science, Northeast University, Shenyang, Liaoning, 110819, People's Republic of China*

[b] *Analytic and Testing center, Research Academy, Northeast University, Shenyang, Liaoning, 110819, People's Republic of China*

*Author to whom correspondence should be addressed.

Tel: +86-024-83684533, Fax: +86-024-83694533.

E-mail: xuxx@mail.neu.edu.cn (Professor X. X. Xu)

xzhang@ mail.neu.edu.cn (Professor X. Zhang).

Abstract

To enhance the photocatalytic property of coordination complex modified polyoxometalate (**CC/POM**) in the visible light region, its nanobelts (**CC/POMNBs**) were loaded on activated carbon fiber (**ACF**) through a simple colloidal blending process. The resulted coordination complex modified polyoxometalate nanobelts loaded activated carbon fiber composite materials (**CC/POMNBs/ACF**) exhibited dramatic photocatalytic activity for the degradation of the rhodamine B (RhB) under visible light irradiation. Optical and electrochemical methods illustrated the enhanced photocatalytic activity of **CC/POMNBs/ACF** originated from high separation efficiency of photogenerated electron and hole on the interface of **CC/POMNBs** and **ACF**, which resulted from the synergy effect between them. In the composite material, the role of **ACF** could be described as photosensitizer and good electron transporter. Furthermore, the influence of mass ratio between **CC/POMNBs** and **ACF** on photocatalytic performance of the resulting composite material was discussed and an ideal value to obtain high efficient photocatalyst had been obtained. The results suggested the loading of **CC/POMNBs** on surface of **ACF** would be a feasible strategy to enhance its photocatalytic activity.

Introduction

Nowadays, critical pollution of organic dyes urges researchers to develop more efficient methods for their treatment.[1, 2] In this field, photocatalysis has received much attention for its ambient operation condition and economic consumption during decomposition of recalcitrant contaminants.[3, 4] As a kind of green and cheap photocatalyst, which possesses similar valence band position and band gap (E_g) with TiO_2, **CC/POM**, especially nanoscale coordination complex modified polyoxometalate (**NCC/POM**) has caught great interests from chemists and is employed to remove organic dyes from waste water.[5, 6] Compared with other POM based photocatalysts, the solubility of **NCC/POM** is much lower, which makes it more convenient in recovering and recycling.[7] Furthermore, **NCC/POM** also exhibits excellent chemical stability during the decomposition of pollutants.[8] Up to now, although some ultraviolet light active **CC/POM** and **NCC/POM** photocatalysts have been explored, the design and fabrication of visible light active **NCC/POM** photocatalysts with high efficiency still remains as a challenge, which impede their further application in waste water treatment.[9] For **NCC/POM** photocatalysts, these drawbacks originate from the wide band gap and the quick recombination rate of photogenerated electron-hole pair during photocatalytic process. Now, the enhancement of photocatalytic activity and efficiency in visible light region become urgent problems in research of **NCC/POM** photocatalyst. To resolve these problems, a feasible strategy is to load **NCC/POM** on a visible light active material, which also possesses excellent photogenerated electron-hole pair separation property.

In this aspect, carbon fiber (**CF**) is an ideal option, which meets all above mentioned requirements perfectly: at first, as a photosensitizer, **CF** can improve the photoresponse of **NCC/POM** in visible light region; secondly, **CF** possesses high

conductivity, which can transport photogenerated electron in time and prevent its recombination with photogenerated hole again; thirdly, its large surface area and excellent absorption capability make it an wonderful carrier for the preparation of composite materials.[10, 11] Although these merits make **CF** a potential choice to improve photocatalytic property of **NCC/POM**, the shortage of active groups (such as -OH and -COOH) on its surface may reduce effective interactions between them and decrease stability of the resulting composite material. To overcome this shortcoming of **CF**, **ACF** is selected as its alternative, because of the existence of a large number of active groups on its surface. Based on these points, **ACF** can not only inherit the advantages of **CF**, but also can form stable composite material with **NCC/POM**. [12-15] Hence we speculate the loading of **NCC/POM** on **ACF** is a feasible strategy is to improve the photocatalytic property of **NCC/POM**.

Our imagination was confirmed to be reasonable by a visible light active photocatalyst **$ZnSiW_{11}$NB/ACF**, which was synthesized by loading the nanobelts of a new **CC/POM**, $[Zn(HPyBim)(SiW_{11}O_{39})]\cdot(H_2PyBim)_2(HPyBim)\cdot(H_2O)_7$ (**$ZnSiW_{11}$**, PyBim = 2-(4-pyridyl)benzimidazole) on surface of **ACF**. Photocatalytic degradation of RhB was investigated and results indicated the loading of **$ZnSiW_{11}$NB** on surface of **ACF** could enhance its photocatalytic activity effectively. To our knowledge, during the fabrication of composite materials, the mass ratio between **$ZnSiW_{11}$NB** and **ACF** (abbreviated as **$ZnSiW_{11}$NB:ACF**) had great effects on optical, electrochemical and photocatalytic property of the resulting composite material. To study the influence of **$ZnSiW_{11}$NB:ACF** value, the fabrication of composite material was conducted under different conditions and an ideal **$ZnSiW_{11}$NB:ACF** value to achieve **$ZnSiW_{11}$NB/ACF** with excellent photocatalytic activity was obtained.

Experimental section

Materials and synthesis

Zinc acetate dehydrate ($Zn(OAc)_2 \cdot 2H_2O$) and tungstosilicic acid hydrate ($H_4SiW_{12}O_{40}$) were obtained from Sinopharm Chemical Reagent Co., Ltd (Shanghai, China). 2-(4-pyridyl)benzimidazole (PyBim) was supplied by Alfa Aesar China Co., Ltd (Tianjin, China). Carbon fiber (**CF**) was purchased from SGL (Germany). All purchased chemicals were of reagent grade and used without further purification. The morphology was observed on an ultra plus field emission scanning electron microscope (ZEISS, Germany). PXRD patterns were recorded on D8 X-ray diffractometer, employing monochromatized Cu Kα incident radiation. FTIR spectra were recorded in the range 4000-400 cm^{-1} on an Alpha Centaur FTIR spectrophotometer using KBr pellets. Diffuse reflectance spectra (DRS) were recorded on a Shimadzu-2501PC spectrometer using $BaSO_4$ as a standard. Electrochemical experiments were conducted on CHI 660B electrochemical workstation. The UV-visible adsorption spectrum was recorded using a Hitachi U-3010 UV-visible spectrometer.

Synthesis of $[Zn(HPyBim)(SiW_{11}O_{39})] \cdot (H_2PyBim)_2(HPyBim) \cdot (H_2O)_7$ **($ZnSiW_{11}$)**

$ZnSiW_{11}$ was prepared from the mixture of $Zn(OAc)_2 \cdot 2H_2O$ (0.022 g, 0.1 mmol), PyBim (0.019 g, 0.1 mmol), $H_4SiW_{12}O_{40}$ (0.288 g, 0.1 mmol), and 6 mL H_2O. The mixture was stirred for 20 minutes and then transferred to a 23 mL Teflon-lined stainless steel bomb and kept at 180˚C under autogenously pressure for 4 days. The reaction system was cooled to room temperature during 24 hours. A large amount of plate yellow crystals of **$ZnSiW_{11}$** were obtained. Yield: 79% (based on Zn).

Synthesis of $ZnSiW_{11}$NB

The crystals of **$ZnSiW_{11}$** were grinded for 3 hours with an agate mortar and pestle. The resulted powder was dissolved in methanol and placed in a Teflon autoclave,

which was heated in a microwave oven at 300 W for 3 hours. The resulted **$ZnSiW_{11}NB$** were separated by centrifugation, rinsed with water and then dried in a vacuum at 80 ˚C for 24 hours.

Synthesis of ACF

CF (1.0 g) was dissolved in 3 M H_2SO_4 aqueous solution (30 ml) at room temperature and dispersed with sonication. After 40 minutes, 3M $(NH_4)_2S_2O_8$ aqueous solution (30 mL) was added slowly to above mixture at room temperature. Then the mixture was sonicated for 2 hours and stirred for 12 hours. The resulted **ACF** was separated and rinsed with water, alcohol and finally dried at 70˚C for 24 hours in a vacuum.

Synthesis of $ZnSiW_{11}NB$/ACF Composite Material

The composite materials were prepared by one-step colloidal blending with **$ZnSiW_{11}NB$** and **ACF** in H_2O. At first, **ACF** was dissolved in 50 mL water. Then, **$ZnSiW_{11}NB$** (4.0 g) was dispersed in water and dropped into the solution of **ACF**. The resulted mixture was sonicated for 2 hours and further stirred for 10 hours at room temperature to obtain a homogeneous solution. The product was separated and dried in a vacuum at 70 ˚C for 10 hours. In the experiment, composite materials were prepared with mass ratio between **$ZnSiW_{11}NB$** and **ACF** equal to 400:1, 200:1, 100:1 and 50:1. These products were labeled as **$ZnSiW_{11}NB$/ACF(A)**, **$ZnSiW_{11}NB$/ACF(B)**, **$ZnSiW_{11}NB$/ACF(C)** and **$ZnSiW_{11}NB$/ACF(D)** respectively.

Synthesis of $ZnSiW_{11}NB$/ACFM

The mixture of **$ZnSiW_{11}NB$** and **ACF** was grinded for 30 minutes with an agate mortar and pestle. The product was separated and rinsed with water, alcohol and finally dried in a vacuum.

X-ray crystallography

Suitable single crystal of **$ZnSiW_{11}$** was carefully selected under an optical microscope and glued on glass fibers. Structural measurements were performed on a Bruker AXS SMART APEX II CCD diffractometer at 293 K. The structures were solved by the direct method and refined by the full-matrix least-squares method on F^2 using the SHELXTL 97 crystallographic software package.[16] Anisotropic thermal parameters were used to refine all non-hydrogen atoms. Carbon-bound hydrogen atoms were placed in geometrically calculated positions; Oxygen-bound hydrogen atoms were located in the difference Fourier maps, kept in that position and refined with isotropic temperature factors. PLATON/SQUEEZE program estimated the solvent-accessible region void to occupy 708.9 $Å^3$ and contain 176.1 electrons. The electron density was modeled as ten water molecules (two water molecules per asymmetric unit) which accounts for 180 electrons. The final chemical formula of $ZnSiW_{11}$ was calculated from the SQUEEZE results combined with the TGA results. The X-ray structural analysis is given in Table S1. Further details of the crystal structure have been deposited to the Cambridge Crystallographic Data Centre as supplementary publication, which can be obtain free of charge (CCDC 955862). The Cambridge Crystallographic Data Centre via www.ccdc.cam.ac.uk/data_request/cif

Wetting behavior test of CF and ACF

A droplet of the sample suspension (**CF** or **ACF**) in ethanol was placed on a cleaned glass substrate fixed on a spin coater at a rotating speed of 1000 rpm for 2 minutes, and a film would be formed after drying. The wettability of the as-prepared films was characterized by measuring the water contact angle (CA) with a contact angle meter. A 2 μL water droplet was placed on this particle array film for water CA measurement. CA values were obtained by averaging five measurements on different areas of the sample surface.

Electrochemical measurements

To prepare the electrodes, 10 mg of the as-prepared samples were dispersed into 5 mL ethanol to give homogeneous suspension upon bath sonication. A 10 μL of the suspension was dip-coated onto ITO and the electrode was then dried at room temperature. Photoelectrochemical tests were carried out with a conventional three-electrode system in quartz cell filled with 0.1 M Na_2SO_4 electrolyte (100 mL) with the **$ZnSiW_{11}$NB/ITO** or **$ZnSiW_{11}$NB/ACF/ITO** electrodes serving as the working electrode, a Pt plate as the counter electrode, and a saturated calomel electrode (SCE) as the reference electrode. Before experiment, the oxygen was excluded completely by N_2. A 300 W xenon lamp were used as the excitation light source for visible irradiation. For incident photon-to-electron conversion efficiency (IPCE) measurements, a mixture solution of 0.05 M I_2 and 0.5 M LiI in propylene carbonate was used as an electrolyte. The monochromatic light was from a 300 W xenon lamp, which passed through a grating monochromator and the wavelength was selected at 5 nm intervals between 280 and 600 nm. Electrochemical impedance spectra (EIS) were recorded in potentiostatic mode. The amplitude of the sinusoidal wave was 10 mV, and the frequency range of the sinusoidal wave was from 100 kHz to 0.05 Hz. The Mott-Schotty plot was measured at a frequency of 100 HZ in the dark.

Photocatalytic property study

The photocatalytic activities of samples were evaluated by the degradation of RhB in the aqueous solution. 80 ml RhB aqueous solution with concentration of 10^{-5} M was mixed with 20 mg catalysts, which was exposed to illumination. Before turning on the lamp, the suspension containing RhB and photocatalyst were magnetically stirred in a dark condition for 40 min till an adsorption-desorption equilibrium was established. Samples were then taken out regularly from the reactor and centrifuged

immediately for separation of any suspended solid. The transparent solution was analyzed by a UV-vis spectrometer. A 300 W medium pressure mercury lamp served as an ultraviolet light source and a 300 W Xe lamp with a cutoff filter ($\lambda \geq 420$ nm) served as a visible light source. Degradation efficiency of RhB was obtained from the following equation: $(C_0 - C)/C_0$ (C_0 is the original concentration of RhB, C is the concentration of RhB after degradation).

Results and discussion

Structure, morphologies and characterization

Single crystal X-ray analysis shows in the fundamental unit of **$ZnSiW_{11}$**, there are three free PyBim ligands, two lattice water molecules and one substituted α-$SiW_{12}O_{40}$ unit (Fig. 1a). As other substituted α-Keggin type POM, in **$ZnSiW_{11}$** one WO_6 octahedron is substituted by $ZnNO_4$ pyramid, in which Zn-N bond distance is 2.107(13) Å and Zn-O bond distances range from 2.030(12) to 2.049(11) Å [18]. The central SiO_4 tetrahedron shares its oxygen atoms with one $\{ZnW_2\}$ and three $\{W_3\}$ groups.[17] These $\{ZnW_2\}$ and $\{W_3\}$ subunits are joined to each other by corner-sharing mode. The Si-O bond distances vary from 1.490(13) to 1.546(15) Å and O-Si-O bond angles are in the range of 107.3(8) to 112.6(8)°. The W-O distances can be divided into three groups: The W-O_t bond distances range from 1.672(11) to 1.728(16) Å, W-$O_{b/c}$ bond distances are in the range of 1.736(12) to 2.077(13) Å and W-O_a bond distance vary from 2.350(14) to 2.500(14) Å. The morphology of **$ZnSiW_{11}$NB** was studied with SEM. It could be seen the thickness of **$ZnSiW_{11}$NB** range from 40 to 60 nm, while its length and width vary from 8 to 12 μm and 1 to 2 μm respectively (Fig. 1b). At low and high magnifications, the surface of **$ZnSiW_{11}$NB** seems very smooth. Thermogravimetric analysis (TGA) of **$ZnSiW_{11}$NB** was carried out in nitrogen gas from 30 to 800 °C (Fig. S1). The first weight loss in the range from 91 to 148 °C is

due to the loss of guest water molecules. The second weight loss from 323 to 452 ℃ can be ascribed to the decomposition of organic ligands.

The activation of **CF** is a very important process for the formation and stability of **$ZnSiW_{11}$NB/ACF**. Although the morphology of **ACF** is similar to that of **CF**, their surface element contents are of great difference (Fig. 2a). The XPS spectra of **CF** and **ACF** were employed to study this point. In **CF**, the peaks located at 284.8 eV and 532.4 eV can be attributed to C1s and O1s respectively.[18] For **ACF**, the intensity of O1s peak increases to a great extent and implies the content of oxygen on its surface is much higher than **CF** (Fig.2b). Furthermore, we also find C1s peaks appear at 286.1 and 288.6 eV, which can be attributed to C-O and C=O (Fig. S2). All these results imply there exist -OH and -COOH groups on surface of **ACF**, which are introduced during activation process of **CF**. This can also be illustrated by the differences between their surface wettabilities. For **CF** and **ACF**, their contact angles are 115.7° and 55.1° respectively, which further imply there exist many hydrophilic groups on the surface of **ACF** (Fig. 2e and 2f). These -OH and -COOH groups can form supramolecular interactions (such as hydrogen bonds) between **$ZnSiW_{11}$NB** and **ACF**, which will "catch" **$ZnSiW_{11}$NB** loaded on the surface of **ACF** and enhance the stability of **$ZnSiW_{11}$NB/ACF**.

The morphologies of **$ZnSiW_{11}$NB/ACF** were also studied with SEM. As for **$ZnSiW_{11}$NB/ACF** composite materials, it can be observed obviously there are different amounts of **$ZnSiW_{11}$NB** on the surface of **ACF** (Fig. 3a to 3d). In these composite materials, the **$ZnSiW_{11}$NB** loaded on **ACF** exhibit similar dimension with **$ZnSiW_{11}$NB** (Fig. 3e to 3f). PXRD was employed to study the structures of **$ZnSiW_{11}$NB** and **$ZnSiW_{11}$NB/ACF** (Fig. 4a). **$ZnSiW_{11}$NB** and **$ZnSiW_{11}$NB/ACF** took on similar diffraction patterns with **$ZnSiW_{11}$**, which illustrates in **$ZnSiW_{11}$NB**

and **$ZnSiW_{11}$NB/ACF** the structures of **$ZnSiW_{11}$** are still retained. Furthermore, no peaks belonging to **ACF** are observed. This can be ascribed to the speculation that the content of **ACF** might be too small to determine. FTIR spectra of **$ZnSiW_{11}$NB/ACF** composite materials were studied to investigate the interactions between **$ZnSiW_{11}$NB** and **ACF** (Fig. 4b). For **$ZnSiW_{11}$NB** the characteristic bands at 784, 921 and 972 cm^{-1} can be attributed to stretching of W=O, W-O and Si-O respectively.[19] Compared with **$ZnSiW_{11}$NB**, in **ACF/$ZnSiW_{11}$NB** composite materials, the stretching of W=O, W-O and Si-O shift to a higher wavenumber region. These reveal in **ACF/$ZnSiW_{11}$NB**, there are effective interactions between **ACF** and **$ZnSiW_{11}$NB**, which can be attributed to hydrogen bond.[20]

Optical property study

The UV-vis diffuse reflectance spectra (DRS) of **$ZnSiW_{11}$NB** and **$ZnSiW_{11}$NB/ACF** composite materials were studied (Fig. S3). Compared with visible light inactive **$ZnSiW_{11}$NB**, **$ZnSiW_{11}$NB/ACF** composite materials exhibit strong absorptions in ultraviolet and visible light region, which suggest **ACF** is a suitable option to extend the photoresponse region of **$ZnSiW_{11}$NB**. To study the influences of **$ZnSiW_{11}$NB:ACF** value on photoresponse region in detail, band gaps (E_g) of all the **$ZnSiW_{11}$NB/ACF** composite materials were obtained from Tauc equation (Fig. 5a). If the mass of **ACF** increased, E_g became smaller at first. But as the mass increased continuously, the value of E_g began growing. In these composite materials, **$ZnSiW_{11}$NB/ACF(C)** possesses the narrowest band gap, which illustrates **$ZnSiW_{11}$NB:ACF** = 100:1 is an optical condition to fabricate composite material with more excellent photoresponse under irradiation of visible light.

Electrochemical analysis

The interface charge separation efficiency can be investigated by photocurrent

spectra, incident photon-to-electron conversion efficiency (IPCE) and electrochemical impedance spectroscopy (EIS). Photocurrent responses of **$ZnSiW_{11}$NB/ITO** and **$ZnSiW_{11}$NB/ACF/ITO** electrodes were studied under visible light irradiation (Fig. 5b). Results indicated the loading of **$ZnSiW_{11}$** on surface of **ACF** can enhance its photocurrent effectively. Furthermore, with the increasing of **$ZnSiW_{11}$:ACF** value, photocurrent of **$ZnSiW_{11}$NB/ACF/ITO** electrode increased at first and then decreased. In all these electrodes, **$ZnSiW_{11}$NB/ACF(C)/ITO** electrode exhibited the largest photocurrent. As photocurrent spectra, after the loading of **$ZnSiW_{11}$NB** on surface of **ACF**, IPCE also enhanced (Fig. 5c). The maximum IPCE value was observed on the **$ZnSiW_{11}$NB/ACF(C)/ITO** (26.78%), which was about 5.80 fold larger than that of **$ZnSiW_{11}$NB/ITO** electrode (4.62%). This further illustrates that a more effective charge separation and transfer process has occurred after **$ZnSiW_{11}$NB** is loaded on surface of **ACF**. To study the charge separation and transfer process in detail, electrochemical impedance spectra (EIS) was employed (Fig. 5d). In EIS, the radius of the *arc* on Nynquist plot reflects the reaction rate occurring at the surface of electrode.[21] The *arc* radius of all **$ZnSiW_{11}$NB/ACF/ITO** electrodes were smaller than **$ZnSiW_{11}$NB/ITO** electrode, which illustrates a more effective separation of photogenerated electron-hole pair as well as a faster interfacial charge transfer have occurred. In all these electrodes, **$ZnSiW_{11}$NB/ACF(C)/ITO** electrode exhibited smallest *arc* radius. This illustrated it possesses the best photogenerated electron-hole pair separation efficiency. In summary, electrochemical tests are well matched with the optical property studies. All these results indicates the loading of **$ZnSiW_{11}$NB** on **ACF** leads to reduction in the recombination rate of photogenerated electron-hole pair and **$ZnSiW_{11}$NB:ACF** = 100:1 is an ideal condition to obtain composite material which possesses better electron-hole pair separation efficiency.

Photocatalytic property study

The photocatalytic activities of **$ZnSiW_{11}NB$** and **$ZnSiW_{11}NB/ACF$** composite materials were evaluated through the degradation of RhB in aqueous solution (Table 1). As an ultraviolet light active photocatalyst, **$ZnSiW_{11}NB$** exhibited no effect on RhB in visible light region (Fig. S4a and 4b). On the contrary, its composite materials with **ACF** showed more excellent photocatalytic activities in visible light region. The photocatalytic efficiency of **$ZnSiW_{11}NB/ACF$** is very close to a well-known POM based visible light active photocatalyst, **CuPW**.[9a] We also observed as the mass of **ACF** increased, photocatalytic efficiency of **$ZnSiW_{11}NB/ACF$** composite materials did not raise monotonously (Fig. 6a and S5). At the beginning, photocatalytic performance enhanced with the increasing of **ACF**, but as **$ZnSiW_{11}NB$:ACF** < 100:1, photocatalytic efficiency began falling down. This can be attributed to the excess of **ACF** may encourage the recombination of photogenerated hole and electron, which may decrease photocatalytic efficiency of the composite materials. So, in **$ZnSiW_{11}NB/ACF(C)$**, the photogenerated electron-hole pair can be separated more effectively and **$ZnSiW_{11}NB$:ACF** = 100:1 is an optical condition to obtain composite material with excellent photocatalytic activity. For **ACF** material based photocatalysts, the enhancement of photocatalytic activity originates from the synergy effect between **ACF** and the other component. As for **$ZnSiW_{11}NB/ACF$**, to illustrate this point clearly, **ACF** and **$ZnSiW_{11}NB/ACFM$** (the mechanically blended products of **$ZnSiW_{11}NB$** and **ACF**) were used as references to evaluate the photocatalytic efficiency (Fig. 6b, S6 and S7). It is notable their photocatalytic properties are weaker than **$ZnSiW_{11}NB/ACF$**, which implies the synergy effect between **$ZnSiW_{11}NB$** and **ACF** that play a crucial role in improving the photocatalytic activity of the **$ZnSiW_{11}NB$**.

In photocatalytic degradation reaction, the activity and stability of recycled catalyst are very important factors to determine the performance of a photocatalyst. Here, photocatalytic properties of **$ZnSiW_{11}NB$/ACF** composite materials were re-examined for five times and recycled photocatalysts still showed excellent catalytic properties (Fig. 6c). Furthermore, the recycled samples also exhibited similar PXRD patterns with original composite materials, which indicated their structures were not destroyed during the photocatalysis decomposition process of RhB (Fig. 6d).

Mechanism study

Mott-Schotty measurement had been applied with impedance technique to study the intrinsic electronic property of **$ZnSiW_{11}NB$/ACF** composite material. We studied the capacitance measurement in the Mott-Schotty-type plot for **$ZnSiW_{11}NB$** (Fig. 7a). The positive slope of the obtained C^{-2}/E plot illustrates **$ZnSiW_{11}NB$** belongs to typical n-type semiconductors. The conductive band potential can also be obtained from this method, which is -0.18 V (vs SCE). Combined with band gap (E_g) estimated from DRS, the valence band (VB) of **$ZnSiW_{11}NB$** is calculated to be 3.00V (vs SCE) according to the formula: $E_{VB} = E_{CB} + E_g$.

Based on the positions of CB, VB and E_g of **$ZnSiW_{11}NB$** and **ACF**, we speculate the mechanism of **$ZnSiW_{11}NB$/ACF** as follows (Fig. 7b). Under irradiation of visible light, **ACF** is excited. Electron is produces on VB orbital of **ACF** and transferred to its CB orbital. After that, electron moves to the CB of **$ZnSiW_{11}NB$**, at the same time, a hole is born on VB of **$ZnSiW_{11}NB$** and inject to VB of **ACF**. This process leads to the charge separation and stabilization, which hinders the recombination of electron and hole. Based on aforementioned points, in **$ZnSiW_{11}NB$/ACF**, the role of **ACF** can be described as photosensitizer and good transportation material of electron.

Conclusion

$ZnSiW_{11}NB/ACF$ composite materials are successfully prepared through the loading of **$ZnSiW_{11}NB$** on surface of activated carbon fiber. We also discuss the influence of **$ZnSiW_{11}NB$:ACF** value on photocatalytic efficiency of the composite material and an optical **$ZnSiW_{11}NB$:ACF** value has been obtained. As expected, compared with **$ZnSiW_{11}NB$**, **ACF** and **$ZnSiW_{11}NB/ACFM$**, **$ZnSiW_{11}NB/ACF$** composite materials exhibit more excellent photocatalytic activity. This enhancement can be attributed to the synergy effect between **$ZnSiW_{11}$** and **ACF**. After comparison of **$ZnSiW_{11}NB/ACF$** and other carbon based composite photocatalytic, such as graphene oxide (GO) or carbon nanotube (CNT) modified TiO_2, we find their degradation efficiency are very close.[22] It can be concluded the preparation of **$ZnSiW_{11}NB/ACF$** enable us to establish a feasible approach to improve photocatalytic property of POM. Furthermore, **$ZnSiW_{11}NB/ACF$** composite material is a new kind of efficient photocatalyst for decontaminating colored wastewater for reuse in industries production.

Acknowledgements

This work was supported by National Natural Science Foundation of China (21303010 and 21103017); Research Foundation for the Doctoral Program of Higher Education of China (20120042110024); Fundamental Research Funds for the Central Universities (N120405005).

Electronic supplementary information (ESI) available: TGA of **$ZnSiW_{11}NB$**; XPS spectrum of **ACF** (C1s peak of **ACF**); DRS of **$ZnSiW_{11}NB$** and **$ZnSiW_{11}NB/ACF$** composite materials; Absorption spectra of RhB degraded with **$ZnSiW_{11}NB$** under irradiation of ultraviolet and visible light; Absorption spectra of RhB degraded with **$ZnSiW_{11}NB/ACF$**, **ACF** and **$ZnSiW_{11}NB/ACFM$** under visible light irradiation.

References

(1) (a) R. Asahi, T. Morikawa, T. Ohwaki, K. Aoki, Y. Taga, *Science* 2001, **293**, 269; (b) W. Zhao, W. H. Ma, C. C. Chen, J. C. Zhao, Z. G. Shuai, *J. Am. Chem. Soc*., 2004, **126**, 4782; (c) Y. Cong, J. L. Zhang, F. Chen, M. Anpo, *J. Phys. Chem. C*, 2007, **111**, 6976.

(2) (a) S. Kohtani, M. Koshiko, A. Kudo, K. Tokumura, Y. Ishigaki, A. Toriba, K. Hayakawa, R. Nakagaki, *Appl. Catal., B*, 2003, **46**, 573; (b) S. Kohtani, M. Tomohiro, K. Tokumura, R. Nakagaki, *Appl. Catal., B*, 2005, **58**, 265.

(3) (a) D. Ravelli, D. Dondi, M. Fagnoni, A. Albini, *Chem. Soc. Rev*., 2009, **38**, 1999; (b) A. Hiskia, A. Mylonas, E. Papaconstantinou, *Chem. Soc. Rev*., 2001, **30**, 62; (c) M. R. Hoffmann, S. T. Martin, W. Y. Choi, D. W. Bahnermann, *Chem. Rev*., 1995, **95**, 69; (d) A. L. Linsebigler; G. Q. Lu, J. T. Yates, *Chem. Rev*., 1995, **95**, 735; (e) T. Hiroaki, F. Musashi, K. Hisayoshi, *Chem. Soc. Rev*., 2011, **40**, 4230.

(4) (a) C. H. Kim, B. H. Kim, K. S. Yang, *Carbon* 2012, **50**, 2472; (b) J. N. Schrauben, R. Hayoun, C. N. Valdez, M. Braten, L. Fridley, J. M. Mayer, *Science* 2012, **336**, 1298; (c) X. Zhang, C. L. Shao, Z. Y. Zhang, J. H. Li, P. Zhang, M. Y. Zhang, J. B. Mu, Z. C. Guo, P. P. Liang, Y. C. Liu, *Appl. Mater. Surf*., 2012, **4**, 785; (d) J. Manna, R. K. Rana, *Chem. Eur. J*., 2012, **18**, 498. (e) Y. Q. Chen, G. R. Li, Y. K. Qu, Y. H. Zhang, K. H. He, Q. Guo, X. H. Bu, *Cryst. Growth Des*., 2013, **13**, 901; (f) Y. Q. Chen, S. J. Liu, Y. W. Li, G. R. Li, K. H. He, Y. K. Qu, T. L. Hu, X. H. Bu, *Cryst. Growth Des*., 2012, **12**, 5426.

(5) (a) D. Lehr, M. Luka, M. R. Wagner, M. Buelger, A. Hoffmann, S. Polarz, *Chem. Mater*., 2012, **44**, 1771; (b) Z. Yang, S. Y. Gao, H. F. Li, R. Cao, *J. Colloid Interface Sci*., 2012, **375**, 172; (c) A. A. Ismail, *Appl. Catal*., *B*, 2012, **117**, 67; (d) S. Civis, M. Ferus, M. Zukalova, P. Kubat, L. Kavan, *J. Phys. Chem. C*, 2012, **116**,

11200.

(6) (a) J. X. Meng, Y. G. Li, H. Fu, X. L. Wang, E. B. Wang, *CrystEngComm*, 2011, **13**, 649; (b) K. Wang, D. D. Zhang, J. C. Ma, P. T. Ma, J. Y. Niu, J. P. Wang, *CrystEngComm*, 2012, **14**, 3205; (c) W. Q. Kan, J. Yang, Y. Y. Liu, J. F. Ma, *Dalton Trans*., 2012, **41**, 11062.

(7) (a) J. X. Meng, Y. Lu, Y. G. Li, H. Fu, X. L. Wang, E. B. Wang, *CrystEngComm*, 2011, **13**, 2479; (b) Y. Ding, J. X. Meng, W. L. Chen, E. B. Wang, *CrystEngComm*, 2011, **13**, 2687; (c) X. L. Wang, Y. F. Wang, G. C. Liu, A. X. Tian, J. W. Zhang, H. Y. Lin, *Dalton Trans*., 2011, **40**, 9299.

(8) (a) J. Y. Niu, S. W. Zhang, H. N. Chen, J. W. Zhao, P. T. Ma, J. P. Wang, *Cryst. Growth Des*., 2011, **11**, 3769; (b) B. F. Meng, W. S. You, X. F. Sun, F. Zhang, M. Y. Liu, *Inorg. Chem. Commun*., 2011, **14**, 35; (c) Y. Q. Jiao, C. Qin, C. Y. Sun, K. Z. Shao, P. J. Liu, P. Huang, K. Zhou, Z. M. Su, *Inorg. Chem. Commun*., 2012, **20**, 273.

(9) (a) H. X. Yang, T. F. Liu, M. N. Cao, H. F. Li, S. Y. Gao, R. Cao, *Chem. Commun*., 2010, **46**, 2429; (b) S. J. Li, S. M. Liu, S. X. Liu, Y. W. Liu, Q. Tang, Z. Shi, S. X. Ouyang, J. H. Ye, *J. Am. Chem. Soc*., 2012, **134**, 19716; (c) P. Huang, C. Qin, Z. M. Su, Y. Xing, X. L. Wang, K. Z. Shao, Y. Q. Lan, E. B. Wang, *J. Am. Chem*., *Soc*., 2012, **134**, 14004; (d) Y. H. Guo, C. W. Hu, *J. Mol. Catal. A: Chem*., 2007, **262**, 136.

(10) (a) S. Kim, S. K. Lim, *Appl. Catal., B*. 2008, **84**, 16; (b) N. K. Dey, M. J. Kim, K. D. Kim, H. O. Seo, D. Kim, Y. D. Kim, D. C. Lim, K. H. Lee, *J. Mol. Catal. A: Chem*., 2011, **337**, 33.

(11) (a) W. Li, Y. Bai, F. J. Li, C. Liu, K. Y. Chan, X. Feng, X. H. Lu, *J. Mater. Chem*., 2012, **22**, 4025; (b) F. J. Li, C. Liu, P. Xu, M. Li, M. H. Zen, S. H. Tang,

Chem. Eng. J., 2014, **243**, 108.

(12) (a) J. W. Shi, J. T. Zheng, P. Wu, X. J. Ji, *Catal. Commun*., 2008, **9**, 1846; (b) J. W. Shi, *Chem. Eng. J*., 2009, **151**, 241.

(13) (a) Y. Z. Zhang, S. H. Deng, B. Y. Sun, H. Xiao, L. Li, G. Yang, Q. Hui, J. Wu, J. T. Zheng, *J. Colloid Interface Sci*., 2010, **347**, 260; (b) G. L. Puma, A. Bono, D. Krishnaiah, J. G. Collin, *J. Hazard. Mater*., 2008, **157**, 209.

(14) (a) H. X. Huang, S. X. Chen, C. Yuan, *J. Power Sources* 2008, **157**, 166; (b) S. H. Yao, J. Y. Li, Z. L. Shi, *Particuology* 2010, **8**, 272.

(15) (a) R. S. Yuan, R. B. Guan, J. T. Zheng, *Scripta Mater*., 2005, **52**, 1329; (b) C. L. Lin, Y. H. Cheng, Z. S. Liu, J. Y. Chen, *J. Hazard. Mater*., 2011, **197**, 254; (c) L. Zhang, Q. Zhou, J. Y. Liu, N. Chang, L. H. Wan, J. H. Chen, *Chem. Eng. J*., 2012, **185-186**, 160.

(16) (a) G. M. Sheldrick, *SHELX-97*, *Program for Crystal Structure Refinement*; University of Göttingen, Germany, 1997; (b) G. M. Sheldrick, *SHELX-97*, *Program for Crystal structure Solution*; University of Göttingen, Germany, 1997.

(17) (a) N. H. Nsouli, E. V. Chubarova, R. Al-Oweini, B. S. Bassil, M. Sadakane, U. Kortz, *Eur. J. Inorg. Chem*., 2013, **SI**, 1742; (b) L. B. Ni, B. Spingler, S. Weyeneth, G. R. Patzke, *Eur. J. Inorg. Chem*., 2013, **SI**, 1681; (c) S. Ogo, S. Moroi, T. Ueda, K. Komaguchi, S. Hayakawa, Y. Ide, T. Sano, M. Sadakane, *Dalton Trans*., 2012, **41**, 9885.

(18) D. Q. Mo, D. Q. Ye, *Surf. Coat. Technol*., 2009, **203**, 1154.

(19) (a) X. L. Hao, Y. Y. Ma, C. Zhang, Q. Wang, X. Cheng, Y. H. Wang, Y. G. Li, E. B. Wang, *CrystEngComm*, 2012, **14**, 6573; (b) S. W. Zhang, J. W. Zhao, P. T. Ma, J. Y. Niu, J. P. Wang, *Chem. Asian J*., 2012, **7**, 966; (c) S. Z. Li, D. D. Zhang, Y. Y. Guo, P. T. Ma, X. Y. Qiu, J. Y. Niu, J. P. Wang, *Dalton Trans*., 2012, **41**, 9885; (d)

J. Zhao, J. S. Wang, J. W. Zhao, P. T. Ma, J. Y. Niu, J. P. Wang, *Dalton Trans*., 2012, **41**, 5832.

(20) (a) S. X. Min, F. Wang, Y. Q. Han, *J. Mater Sci*., 2007, **42**, 9966; (b) J. H. Wei, Q. Zhang, Y. Liu, R. Xiong, C. X. Pang, J. Shi, *J. Nanopart. Res*., 2011, **15**, 3157; (c) S. De, A. Dey, S. K. De, *J. Phys. Chem. Solids*, 2007, **68**, 66; (d) L. X. Zhang, P. Liu, Z. X. Su, *Polym. Degrad. Stab*., 2006, **91**, 2213.

(21) (a) H. Liu, S. A. Cheng, M. Wu, H. J. Wu, J. Q. Zhang, W. Z. Li, C. N. Cao, *J. Phys. Chem. A,* 2000, **104**, 7016; (b) W. H. Leng, Z. Zhang, J. Q. Zhang, C. N. Cao, *J. Phys. Chem. B,* 2005, **109**, 15008.

(22) (a) P. Song, X. Y. Zhang, M. X. Sun, X. L. Cui, Y. H. Lin, *Nanoscale* 2012, **4**, 1800; (b) T. D. Nguyen-Phan, V. H. Pham, E. W. Shin, H. D. Pham, S. Kim, J. S. Chung, E. J. Kim, S. H. Hur, *Chem. Eng. J*., 2011, **170**, 226.

Table 1 Degradation efficiency of RhB with different photocatalysts

Photocatalyst	Condition	T (hours)	η (%)
$ZnSiW_{11}NB$	ultraviolet light irradiation	6	55.53
$ZnSiW_{11}NB$	visible light irradiation	6	2.51
$ZnSiW_{11}NB$/ACF(A)	visible light irradiation	6	81.30
$ZnSiW_{11}NB$/ACF (B)	visible light irradiation	4	83.37
$ZnSiW_{11}NB$/ACF (C)	visible light irradiation	2	89.36
$ZnSiW_{11}NB$/ACF (D)	visible light irradiation	5	85.68
ACF	visible light irradiation	6	33.57
$ZnSiW_{11}NB$/ACF(A)M	visible light irradiation	6	13.99
$ZnSiW_{11}NB$/ACF(B)M	visible light irradiation	6	22.03
$ZnSiW_{11}NB$/ACF(C)M	visible light irradiation	6	37.01
$ZnSiW_{11}NB$/ACF(D)M	visible light irradiation	6	53.39

Figure Captions

Figure 1 (a) The fundamental unit of **$ZnSiW_{11}$**; (b) SEM of **$ZnSiW_{11}$NB** in high magnification.

Figure 2 (a) SEM of **CF**; (b) SEM of **ACF**; (c) XPS spectrum of **CF**; (d) XPS spectrum of **ACF**; (e) The shape of a water droplet on the surface of **CF**; (f) The shape of a water droplet on the surface of **ACF**.

Figure 3 (a) SEM of **$ZnSiW_{11}$NB/ACF(A)**; (b) SEM of **$ZnSiW_{11}$NB/ACF(B)**; (c) SEM of **$ZnSiW_{11}$NB/ACF(C)**; (d) SEM of **$ZnSiW_{11}$NB/ACF(D)**; (e)SEM of **$ZnSiW_{11}$NB/ACF(A)** in high magnification image; (f) SEM of **$ZnSiW_{11}$NB/ACF(B)** in high magnification image; (g) SEM of **$ZnSiW_{11}$NB/ACF(C)** in high magnification image; (h) SEM of **$ZnSiW_{11}$NB/ACF(D)** in high magnification image.

Figure 4 (a) PXRD patterns of **$ZnSiW_{11}$NB**, **ACF** and **$ZnSiW_{11}$NB/ACF**; (b) FTIR of **$ZnSiW_{11}$NB/ACF**.

Figure 5 (a) Tauc plots **$ZnSiW_{11}$NB/ACF**; (b) Photocurrent spectra of **$ZnSiW_{11}$NB** and **$ZnSiW_{11}$NB/ACF** under visible light irradiation; (c) IPCE of **$ZnSiW_{11}$NB** and **$ZnSiW_{11}$NB/ACF**; (d) EIS of **$ZnSiW_{11}$NB** and **$ZnSiW_{11}$NB/ACF**.

Figure 6 (a) Degradation rate for RhB by **$ZnSiW_{11}$NB** and **$ZnSiW_{11}$NB/ACF** under visible light; (b) Degradation rate for RhB by **$ZnSiW_{11}$NB/ACFM** under visible light; (c) Cycling runs of the degradation of RhB in the presence of **$ZnSiW_{11}$NB/ACF**; (d) PXRD of recycled **$ZnSiW_{11}$NB/ACF**.

Figure 7 (a) Mott-Schotty plot of **$ZnSiW_{11}$NB**. (b) Diagram of the photocatalytic mechanism for **$ZnSiW_{11}$NB/ACF** under visible light irradiation.

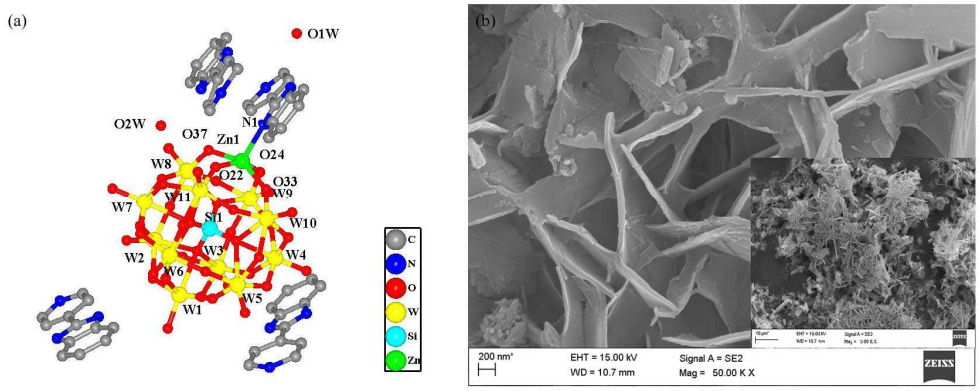
(a)
O1W
O2W
O37
Zn1
N1
O24
W8
O22
O33
W9
W7
W11
Si1
W10
W2
W3
W4
W6
W5
W1
C
N
O
W
Si
Zn
(b)
200 nm
EHT = 15.00 kV
WD = 10.7 mm
Signal A = SE2
Mag = 50.00 K X
ZEISS

Figure 1

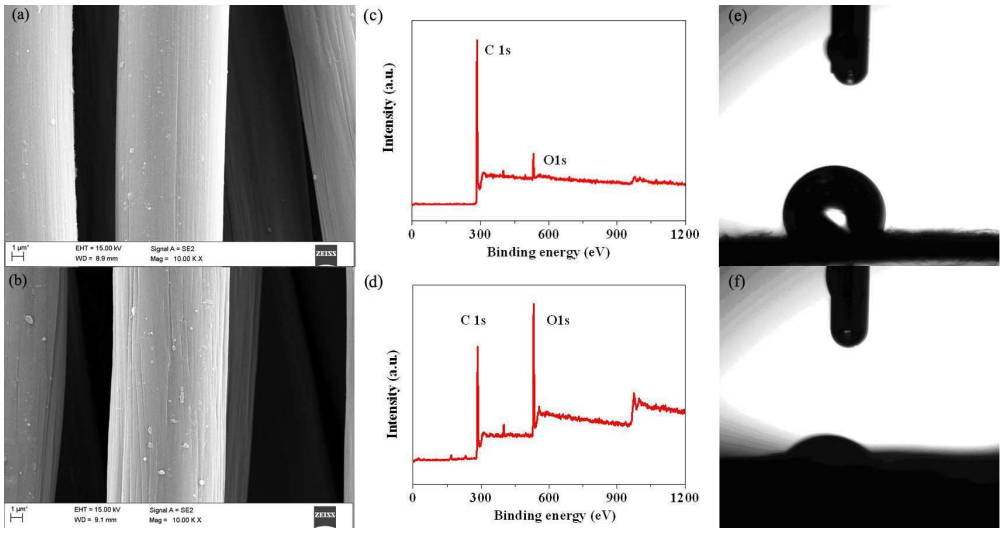
(a)
(b)
(c)
C 1s
O1s
Intensity (a.u.)
0
300
600
900
1200
Binding energy (eV)
(d)
C 1s
O1s
Intensity (a.u.)
0
300
600
900
1200
Binding energy (eV)
(e)
(f)

Figure 2

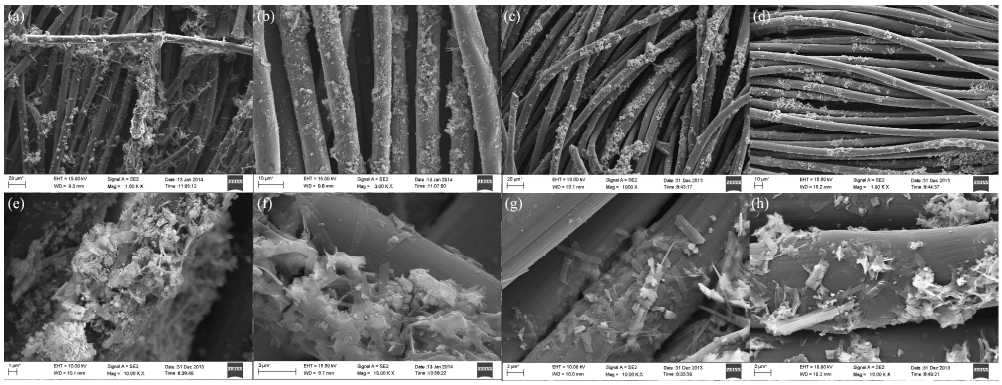

Figure 3

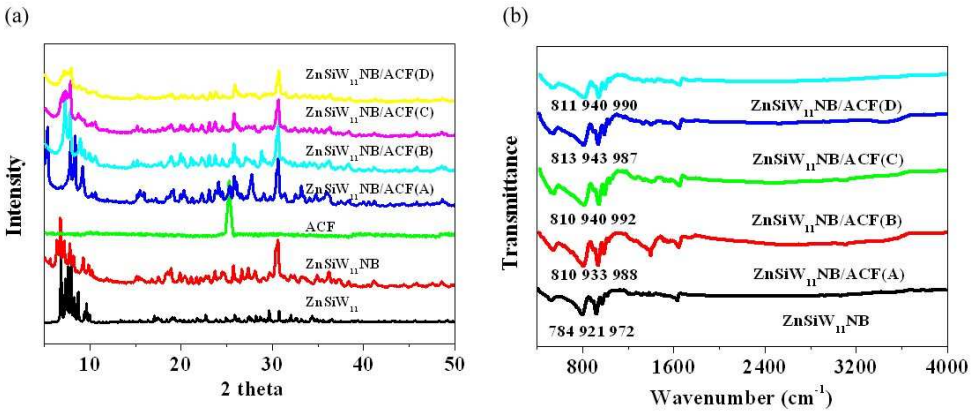
(a)
(b)
Intensity
2 theta
10
20
30
40
50
ZnSiW11NB/ACF(D)
ZnSiW11NB/ACF(C)
ZnSiW11NB/ACF(B)
ZnSiW11NB/ACF(A)
ACF
ZnSiW11NB
ZnSiW11
Transmittance
Wavenumber (cm-1)
800
1600
2400
3200
4000
811 940 990
813 943 987
810 940 992
810 933 988
784 921 972

Figure 4

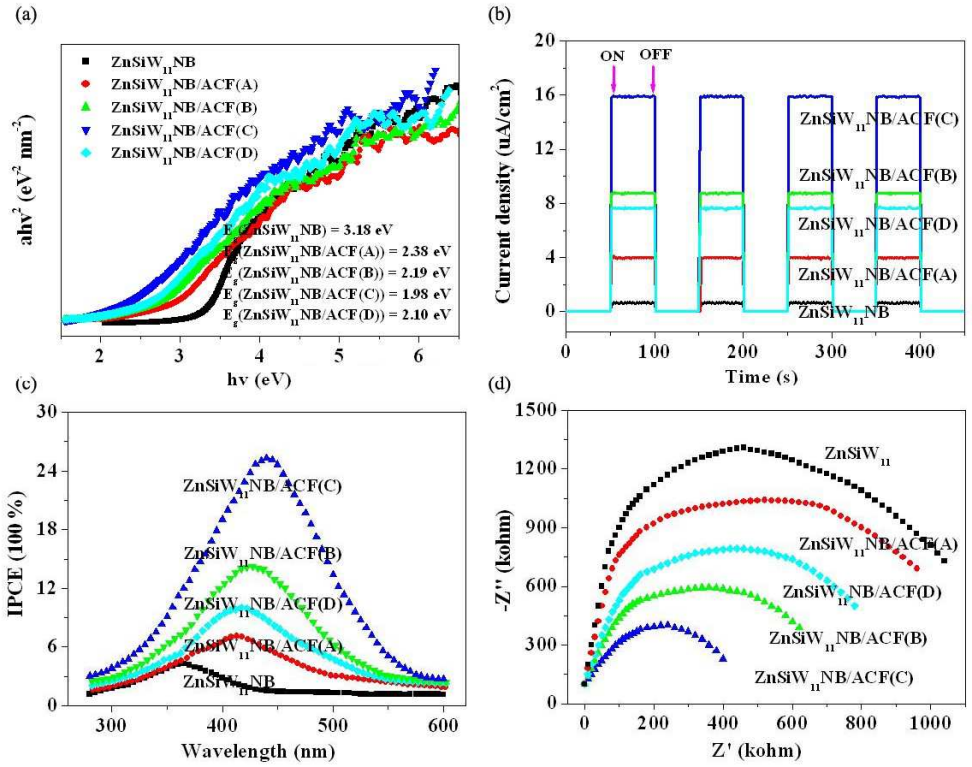
(a)
ZnSiW11NB
ZnSiW11NB/ACF(A)
ZnSiW11NB/ACF(B)
ZnSiW11NB/ACF(C)
ZnSiW11NB/ACF(D)
Eg(ZnSiW11NB) = 3.18 eV
Eg(ZnSiW11NB/ACF(A)) = 2.38 eV
Eg(ZnSiW11NB/ACF(B)) = 2.19 eV
Eg(ZnSiW11NB/ACF(C)) = 1.98 eV
Eg(ZnSiW11NB/ACF(D)) = 2.10 eV
ahv2 (eV2 nm-2)
hv (eV)
(b)
ON
OFF
ZnSiW11NB/ACF(C)
ZnSiW11NB/ACF(B)
ZnSiW11NB/ACF(D)
ZnSiW11NB/ACF(A)
ZnSiW11NB
Current density (uA/cm2)
Time (s)
(c)
ZnSiW11NB/ACF(C)
ZnSiW11NB/ACF(B)
ZnSiW11NB/ACF(D)
ZnSiW11NB/ACF(A)
ZnSiW11NB
IPCE (100 %)
Wavelength (nm)
(d)
ZnSiW11
ZnSiW11NB/ACF(A)
ZnSiW11NB/ACF(D)
ZnSiW11NB/ACF(B)
ZnSiW11NB/ACF(C)
-Z'' (kohm)
Z' (kohm)

Figure 5

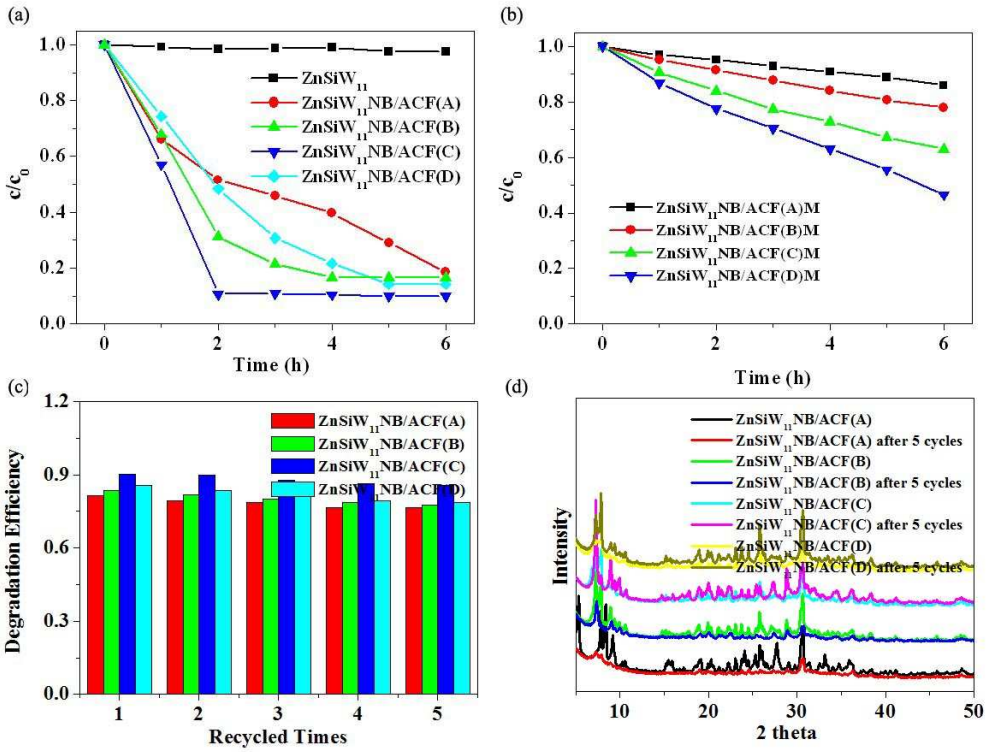
(a)
c/c0
Time (h)
ZnSiW11
ZnSiW11NB/ACF(A)
ZnSiW11NB/ACF(B)
ZnSiW11NB/ACF(C)
ZnSiW11NB/ACF(D)
(b)
c/c0
Time (h)
ZnSiW11NB/ACF(A)M
ZnSiW11NB/ACF(B)M
ZnSiW11NB/ACF(C)M
ZnSiW11NB/ACF(D)M
(c)
Degradation Efficiency
Recycled Times
ZnSiW11NB/ACF(A)
ZnSiW11NB/ACF(B)
ZnSiW11NB/ACF(C)
ZnSiW11NB/ACF(D)
(d)
Intensity
2 theta
ZnSiW11NB/ACF(A)
ZnSiW11NB/ACF(A) after 5 cycles
ZnSiW11NB/ACF(B)
ZnSiW11NB/ACF(B) after 5 cycles
ZnSiW11NB/ACF(C)
ZnSiW11NB/ACF(C) after 5 cycles
ZnSiW11NB/ACF(D)
ZnSiW11NB/ACF(D) after 5 cycles

Figure 6

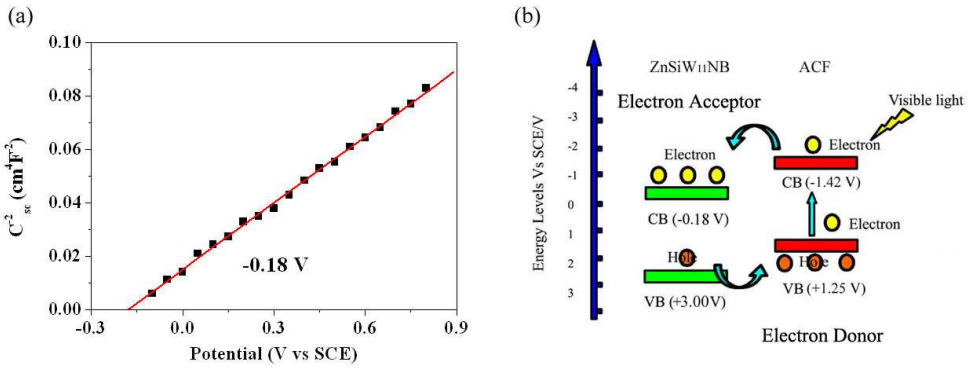
(a)
0.10
0.08
0.06
0.04
0.02
0.00
-0.3
0.0
0.3
0.6
0.9
Potential (V vs SCE)
-0.18 V
(b)
ZnSiW11NB
ACF
Electron Acceptor
Visible light
Electron
Electron
CB (-1.42 V)
CB (-0.18 V)
Electron
Hole
Hole
VB (+1.25 V)
VB (+3.00V)
Energy Levels Vs SCE/V
-4
-3
-2
-1
0
1
2
3
Electron Donor

Figure 7